

Tunable Plasmonic Induced Transparency in Graphene Nanoribbon Resonators

Huawei Zhuang*, Hongkui Xu, Shulan Gong, and Yuling Wang

Abstract—A plasmonic induced transparency (PIT) structure is proposed and numerically investigated using the finite difference time domain (FDTD) method, which is achieved by the destructive interference between two graphene nanoribbon resonators and a bus waveguide. The common three-level atom system is used to explore the physical origin of the PIT behavior. The simulation results show that the PIT effect at different modes can be excited or suppressed by choosing the proper coupling position of the resonators. The peak and bandwidth of the transparent window are controlled by the coupling distance between the resonators and the bus waveguide, and the position of the transparent window can be freely tuned by adjusting the chemical potential of graphene. The proposed PIT structure may offer a new avenue for novel integrated optical switching and slow-light devices in THz and mid-infrared frequencies.

1. INTRODUCTION

Electromagnetically induced transparency (EIT) is a special and counterintuitive phenomenon which occurs in atomic systems due to the quantum destructive interference between the excitation pathways to the atomic upper level [1, 2]. The sharp transparency window with narrow spectral width will produce a variety of novel effects [3]. Even though, the operating conditions of the atomic systems need low-temperature environments and stable gas lasers, which severely hamper the realization of the quantum EIT effect [4]. To overcome these drawbacks, a series of new mechanisms are proposed to mimic the traditional atomic system, such as metamaterial induced transparency [5, 6], coupled-resonator-induced transparency [7, 8], and plasmon-induced transparency (PIT) [9]. Recently, the PIT structure using noble metal [10, 11] has attracted increasing attentions, because surface plasmon polaritons (SPPs) is easily excited at the surface of noble metal, which can overcome the traditional diffraction limit at sub-wavelength regions. In addition, the metal metamaterial structure can also induce the localized resonance, which can be used as absorber or sensor [12–14]. Because the permittivity of noble metal cannot be tuned freely, the tunability of PIT structure fabricated with noble metals is hampered once the geometry of the structure is fixed.

As a single monolayer of sp^2 hybridized carbon, graphene has attracted great interest due to its excellent electrical and optical properties. Like the noble metal material, graphene also has the ability to support SPPs [15, 16]. The effective index of graphene SPPs can attain to ~ 100 in the mid-infrared region, comparing to a typical value of ~ 1.03 for SPPs on metals [17]. Meanwhile, when the width of graphene ribbon decreases to tens of nanometers, only edge mode leaves, which is more suitable for the electromagnetic coupling between the adjacent elements [18–20]. Due to the above advantages, more attentions have been focused on investigating tunable EIT-like structures based on graphene, which is usually achieved by two kinds of means: the bright-dark mode coupling [21–24] and the bright-bright

Received 24 March 2017, Accepted 4 June 2017, Scheduled 14 June 2017

* Corresponding author: Huawei Zhuang (zhuanghuawei@sdjzu.edu.cn).

The authors are with the School of Information & Electrical Engineering, Shandong Jianzhu University, Jinan 250101, China.

mode coupling [25]. To the best of our knowledge, how to excite or suppress the PIT at different resonant modes has not been studied yet.

In this paper, we use two graphene nanoribbon resonators as excited state and metastable state to realize PIT effect, which can be explained by the common energy diagram of three-level atomic systems. The novelty of this paper is that the PIT at different resonant modes can be excited or suppressed by choosing the proper distance of the resonator (metastable state) along the reference plane. Numerical results show that the peak of the transmission window can be controlled by changing the coupling distance between the two nanoribbon resonators, and the transparent window is freely tuned at will by adjusting the chemical potential of the resonators.

2. THEORETIC ANALYSIS OF THE COUPLING BETWEEN TWO GRAPHENE RESONATORS

At THz and mid-infrared frequencies, the surface conductivity of graphene is usually expressed by the semi-metal conductivity model. At room temperature, the intraband transition dominates, and the Kubo formula is reduced to [26, 27]

$$\sigma_g = \frac{ie^2\mu_c}{\pi\hbar^2(\omega + i\tau^{-1})}, \quad (1)$$

where e is the electron charge, $\hbar = h/2\pi$ the reduced Plancks constant, ω the angular frequency, μ_c the chemical potential of graphene, and τ the relaxation time. The value of τ is set as 0.3 ps, which is in agreement with the measured, impurity sample. In the 3D FDTD simulations, the equivalent permittivity of graphene follows by $\varepsilon_{eq} = \varepsilon_0 + i\sigma_g/(\omega\Delta)$, where ε_0 is the permittivity of free space, and Δ is the thickness of graphene nanoribbon.

In this paper, a graphene-based PIT structure is proposed, and the 3D diagram and its top view are plotted in Figs. 1(a) and (b), respectively. Fig. 1(c) shows the back-gate structure with a gating voltage applied between the Cr/Au gating pad and the Si substrate, which is used to tune the chemical potential of graphene. The permittivity of SiO₂ and Si substrate are 2.09 and 11.9, and the thickness of SiO₂ layer is set as $h = 50$ nm. This device can be realized by the chemical vapor deposition, electron-

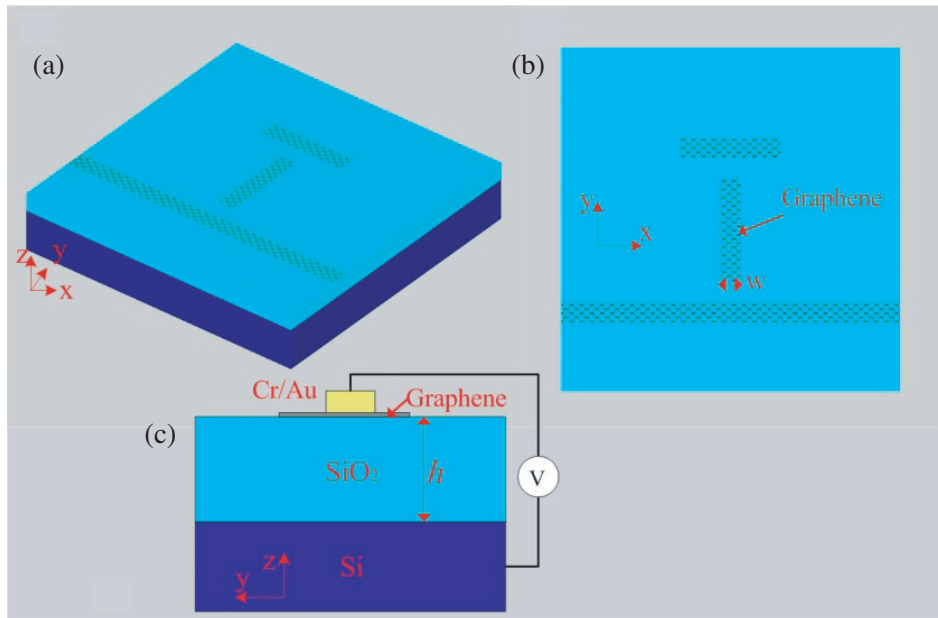


Figure 1. (a) 3D diagram. (b) Top view of the proposed PIT structure. (c) Side view of graphene nanoribbon deposited on the SiO₂/Si substrate. A gating voltage is applied between the Cr/Au gating pad and the Si substrate.

beam lithography and etching method. The width of graphene is set as $w = 20$ nm, which can only support graphene SPPs edge mode. Compared to waveguide modes, edge modes have a relatively higher effective index [18], which can make the plasmonic device more compact than that with the waveguide modes.

Figure 2(a) illustrates the schematic of the proposed PIT structure investigated in this paper. The main structural parameters are the width of the graphene nanoribbon (including the bus waveguide, resonator R_1 and R_2) (w), the length of the resonator R_1 and R_2 (L_1 and L_2), the distance between the resonators R_1 and R_2 (t), and the distance between the bus waveguide and resonators R_1 (d). In our simulations, the thickness of graphene is set as $\Delta = 0.34$ nm, which is the value of a single-layer-atom thickness. In order to save storage space and computing time, non-uniform mesh is applied in the FDTD simulation. The minimum mesh size in the z direction is set as 0.034 nm, and $1 \text{ nm} \times 1 \text{ nm}$ is set at the x and y directions. The simulation is under perfectly matched layer (PML) with a dipole source placed on the left side of the bus waveguide to excite the graphene SPPs edge mode. As shown in Fig. 2(a), two monitors are set at the lines of SPP_{in} and SPP_{out} to detect the incident power P_{in} and transmitted power P_{out} . The transmission is defined as $T = P_{\text{out}}/P_{\text{in}}$.

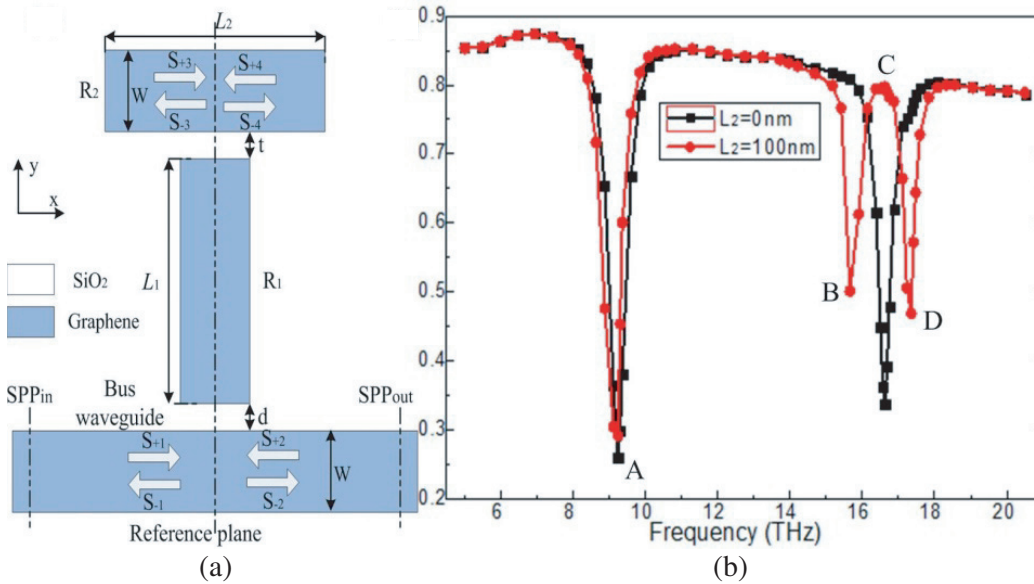


Figure 2. (a) Schematic of the graphene nanoribbon PIT structure. (b) Transmission spectra of the PIT structure with $L_1 = 100$ nm and $L_2 = 0$ nm, 100 nm respectively.

The transmission spectra of the resonator system with $L_1 = 100$ nm and $L_2 = 0$ nm, 100 nm are shown in Fig. 2(b). The other geometric parameters are set as $w = 20$ nm, $t = d = 5$ nm, and $\mu_c = 0.15$ eV. The transmission spectrum at $L_1 = 100$ nm and $L_2 = 0$ nm in Fig. 2(b) shows two obvious transmission dips lie at $f = 9.072$ THz and 16.580 THz, corresponding to the first and second resonant modes. The corresponding E_z field distributions are shown in Figs. 3(a) and (b), from which we can obviously observe one and two wave nodes in the standing wave distribution. When the length of resonator R_2 increases to $L_2 = 100$ nm, the spectrum at mode 1 keeps almost unchanged compared with $L_2 = 0$ nm; but the spectrum at mode 2 exhibits a narrow transmission peak shown in Fig. 2(b), which demonstrates the PIT effect. The transmission peak can reach as high as 0.80 at the frequency of 16.580 THz.

Why do the two modes demonstrate different transmission characteristics at $L_2 = 100$ nm? As we know, the wave node in the standing wave distribution for mode 1 is located in the center of the resonator R_2 . As a type of electromagnetic wave, the SPPs edge mode has the form of $\exp(-i\omega t + i\beta x)$, assuming the SPPs travel along the $+x$ direction. Here, we set Φ as the phase difference of a round trip in the resonator R_2 . When the resonance condition $\Phi = 2\beta L = 2m\pi$ is satisfied, the stable standing waves can be excited within R_2 . As shown in Fig. 2(a), the waves in the resonator should satisfy a

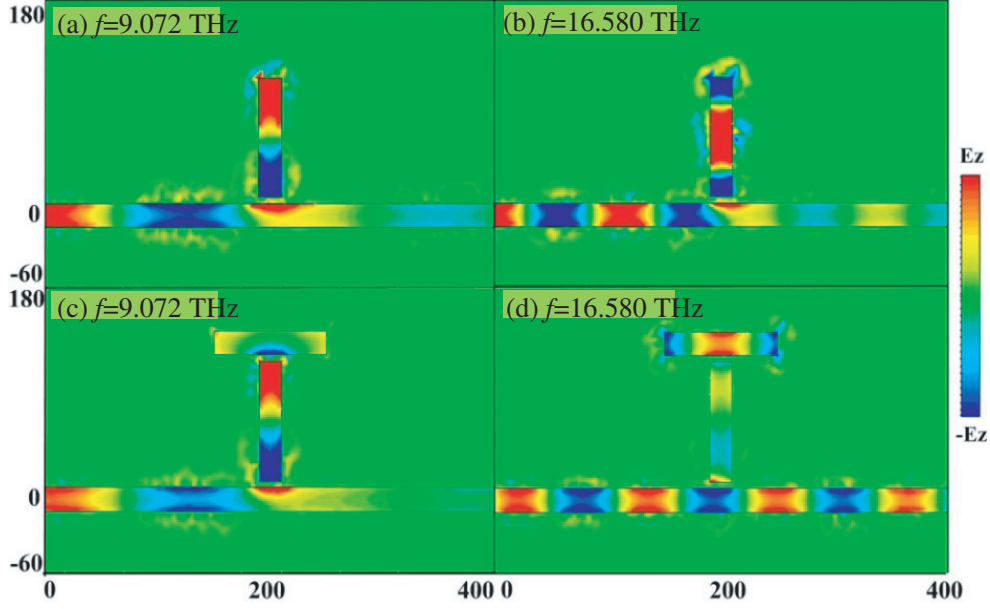


Figure 3. The E_z field distribution at $L_2 = 0$ nm for the (a) first mode, (b) second mode and $L_2 = 100$ nm corresponding to the (c) first mode, (d) second mode.

steady-state relationship of $S_{+3} \approx S_{-3}\sigma e^{im\pi}$ and $S_{+4} \approx S_{-4}\sigma e^{im\pi}$. Here, σ is the attenuation term of the SPP mode during a half round trip in the right (or left) side from the reference plane, respectively. In order to simplify the analysis the attenuation term is set as $\sigma \approx 1$. Thus, the relationship of $S_{+3} \approx S_{-3}\sigma e^{i\pi} = -S_{-3}$ and $S_{+4} \approx -S_{-4}$ satisfies in the first mode at $m = 1$. As shown in Fig. 3(c), the two parts $S_{\pm i}$ ($i = 3, 4$) at resonator R_2 cancel each other along the reference plane with little energy coupling between R_1 and R_2 , resulting in no PIT appearing in the first mode. If we want to excite PIT in the first mode, one has to shift the coupling position over a distance along the reference plane for the resonator R_2 , which will be discussed in the following chapters. On the contrary, $S_{+3} \approx S_{-3}$ and $S_{+4} \approx S_{-4}$ satisfies due to $\beta L = 2\pi$ for the second mode. Then, the energy can be easily coupled between R_1 and R_2 , and the destructive interference from the coupling of the two resonators results in the PIT effect, as shown in Figs. 2(b) and 3(d).

A common three-level plasmonic system structure [5] is used to explore the physical origin of PIT, as shown in Fig. 4(a). The graphene bus waveguide is considered as the ground state $|1\rangle$. The resonator R_1 is directly excited by the near-field coupling and acts like an excited state $|3\rangle$. The resonator R_2 cannot be directly excited by the bus waveguide and the only means to excite R_2 is by the evanescent coupling from R_1 , so it acts like a metastable state $|2\rangle$. The transparent window is the result of extreme destructive interference between two propagation pathways: $|1\rangle\text{-}|3\rangle\text{-}|2\rangle\text{-}|3\rangle$ and $|1\rangle\text{-}|3\rangle$, which allows the incident SPPs to propagate through the structure uninhibited. At the same time, we can see that the electrical field in R_1 is cancelled, and it is enhanced in R_2 , which cancels the original resonance effect at the transmission dip and leads to the formation of the PIT effect observed, as shown in Fig. 2(b). In other words, the destructive interference will split into two dressed states resulting in the ground state being excited to either $|+\rangle$ or $|-\rangle$ shown in Fig. 4(b), corresponding to the frequencies f_- and f_+ . The bandwidth of the transparency window can be expressed as $\Delta f = f_+ - f_-$. The transmission spectra of the two transmission dips at $f_- = 15.774$ THz and $f_+ = 17.249$ THz are presented in Figs. 4(c)–(d). It is quite obvious that both the two resonators are strongly excited at the two transmission dips due to most of the SPPs edge modes confined and trapped in R_1 and R_2 . The E_z field distributions of the two resonators are in-phase at $f_+ = 17.249$ THz while at $f_- = 15.774$ THz are out-of-phase. In addition, from Fig. 2(b) we can see that transmission value at f_+ is lower than that at f_- at $t = 5$ nm. This is because different phase coupling modes at f_- and f_+ will produce different electromagnetic field distributions around R_1 and R_2 .

As stated earlier, the PIT effect cannot be excited at the first mode. In order to induce the PIT

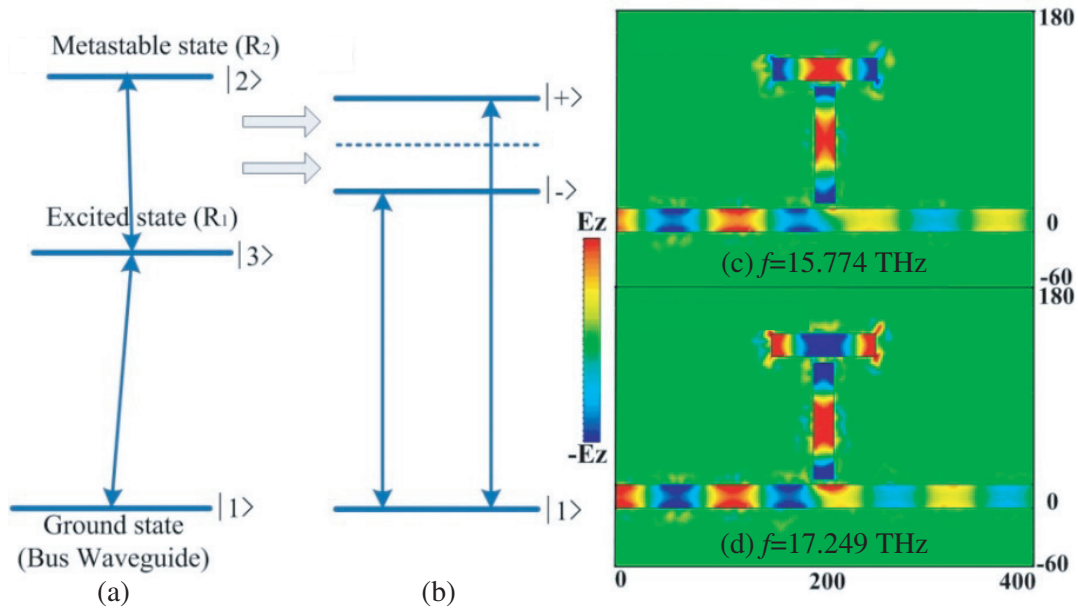


Figure 4. (a) A common three-level plasmonic system. (b) The destructive interference makes the system split into two dressed states $|+\rangle$ or $|-\rangle$ corresponding to the E_z field distribution at $f =$ (c) 15.774 THz (d), 17.249 THz.

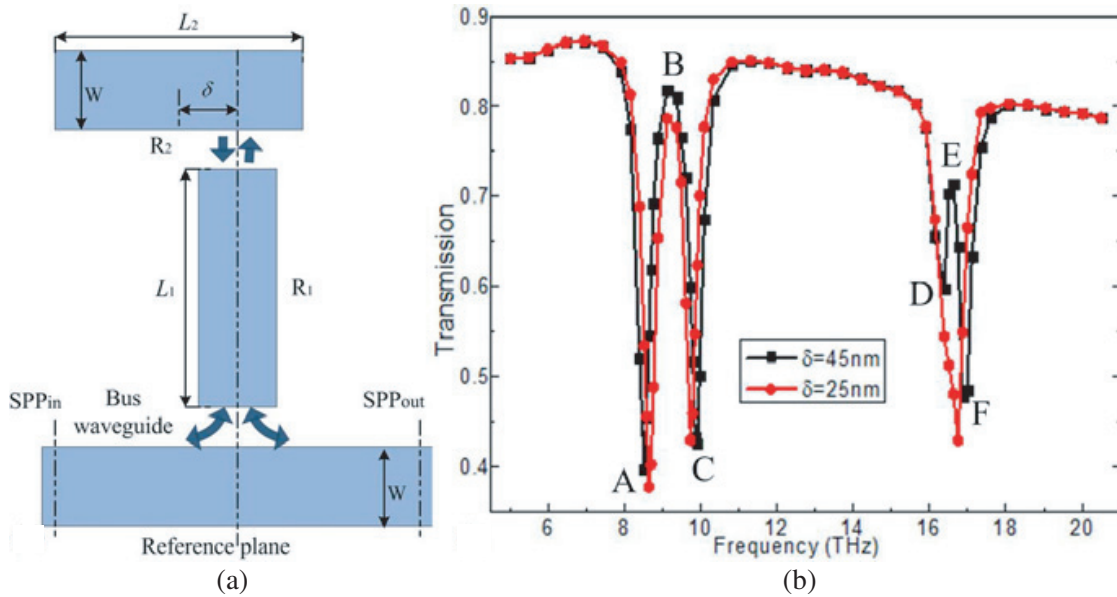


Figure 5. (a) Schematic diagram of the PIT structure with a distance away from the reference plane. (b) Transmission spectra of the PIT structure with the distance of 25 nm and 45 nm, respectively.

in the first mode, one has to shift the coupling position over a distance away from the reference plane. Fig. 5(a) shows the schematic of the PIT structure with a distance δ away from the reference plane, and the corresponding transmission spectra at $\delta = 25$ nm and 45 nm are demonstrated in Fig. 5(b). It is obvious that at $\delta = 25$ nm only the first mode appeared in the spectrum, but the 2nd mode kept the original transmission effects, because the relationship of $S_{+3} \approx S_{-3}$ and $S_{+4} \approx S_{-4}$ satisfies in the first mode and $S_{+3} \approx -S_{-3}$ and $S_{+4} \approx -S_{-4}$ in the second mode. Figs. 6(a)–(c) give the E_z field distribution of the PIT structure corresponding to points A, B, and C in Fig. 5(b) at $\delta = 25$ nm. At

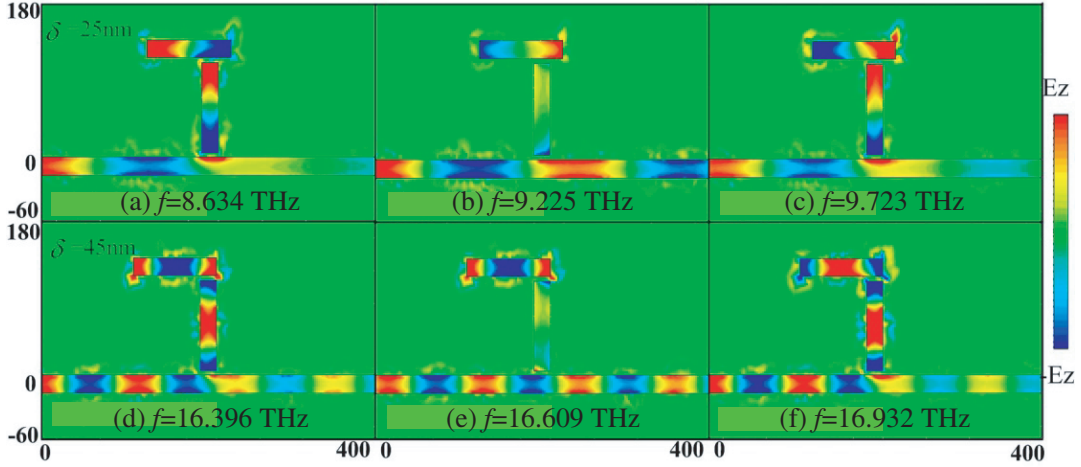


Figure 6. E_z field distribution at the distance of (a)–(c) 25 nm corresponding to points A–C in Fig. 5(b), (d)–(f) 45 nm corresponding to points D–F in Fig. 5(b).

$\delta = 45$ nm, the above relationship cannot be satisfied, so the PIT effect is excited simultaneously at the two modes, which is verified by the black line of Fig. 5(b). The E_z field distribution at the transparent window for the second mode at $\delta = 45$ nm is shown in Figs. 6(d)–(f), which is corresponding to points D, E, and F of the black line. In conclusion, by adjusting the proper distance δ away from the reference plane, the PIT effect can be excited at either mode or two modes simultaneously.

3. PERFORMANCE ANALYSIS OF THE PIT AT DIFFERENT PARAMETERS

In order to evaluate the performance of the proposed PIT structure, the coupling distance t and d are the important parameters influencing the transparent window at the resonant modes. As shown in Fig. 7(a), the transmission peaks of the transparent window are decreased with the increasing of the coupling distance t . At the same time, when the coupling distance t is increased from 5 nm to 15 nm, the coupling between R_1 and R_2 weakens and the bandwidth between f_- and f_+ becomes smaller. On the contrary, when we only change the distance d with other parameters unchanged, only the transmission peak decreases with the bandwidth of the window unchanged, as shown in Fig. 7(b).

Of all the factors determining the graphene characteristics, the chemical potential μ_c is the most commonly used, since it can be easily tuned by the back-gate structure shown in Fig. 1(c). Thus, the position of the transparent window can be tuned by changing the chemical potential of graphene. Firstly, the chemical potential of R_1 and R_2 are set as the same values (i.e., $\mu_{cR1} = \mu_{cR2}$). Fig. 8(a) shows the transmission spectra for the resonators with $\mu_{cR1} = \mu_{cR2}$ varying from 0.15 to 0.18 eV, from which we can see that the transparent window shows blue shift with the increase of the chemical potential. Because the effective index of graphene SPPs increases with the increasing of the chemical potential [28], resulting in the resonant frequency of R_1 and R_2 increasing. Next, we set the two resonators with different chemical potentials, and Fig. 8(b) gives the transmission spectra at the chemical potential of 0.15 and 0.165 eV. Compared with the chemical potential fixed at 0.15 eV, the transparency window is also blue-shifted with one of the two chemical potentials increasing. At the same time, due to the existence of the discrepancy in chemical potential, the difference between the two transmission dips enlarges with a highly asymmetric spectrum, as shown in Fig. 8(b). In fact, increasing chemical potential discrepancy between R_1 and R_2 may transform an PIT spectrum to detuned Fabry-Perot resonators with the transmission peak occurring at the intermediate resonant frequencies [29]. In order to verify the above analysis, the simulation results show that the transmission peak frequency at $\mu_{cR1} = \mu_{cR2} = 0.15$ eV is 16.62 THz at mode 2, comparing to 16.81 THz at $\mu_{cR1} = 0.165$ eV, $\mu_{cR2} = 0.15$ eV, as well as 17.11 THz at $\mu_{cR1} = 0.15$ eV, $\mu_{cR2} = 0.165$ eV. It is clearly seen that the transparency window can be shifted over a broad range in the investigated frequency regime by the method of gating voltage, which is difficult to achieve in conventional noble metal plasmonic devices.

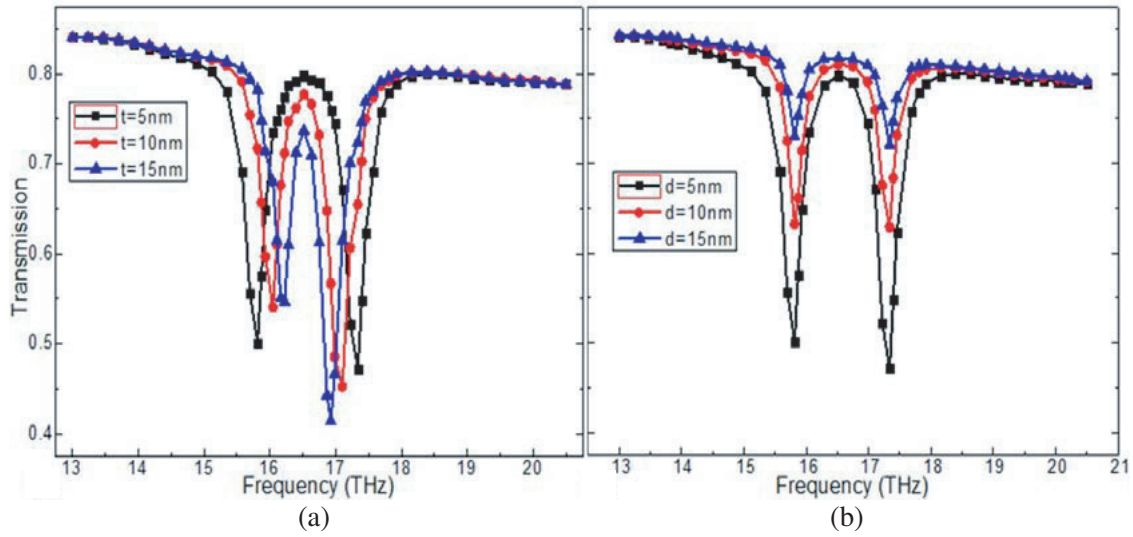


Figure 7. Transmission spectra at the coupling distance of (a) $t = 5, 10,$ and 15 nm. (b) $d = 5, 10,$ and 15 nm. The other parameters are $L_1 = L_2 = 100$ nm, $w = 20$ nm.

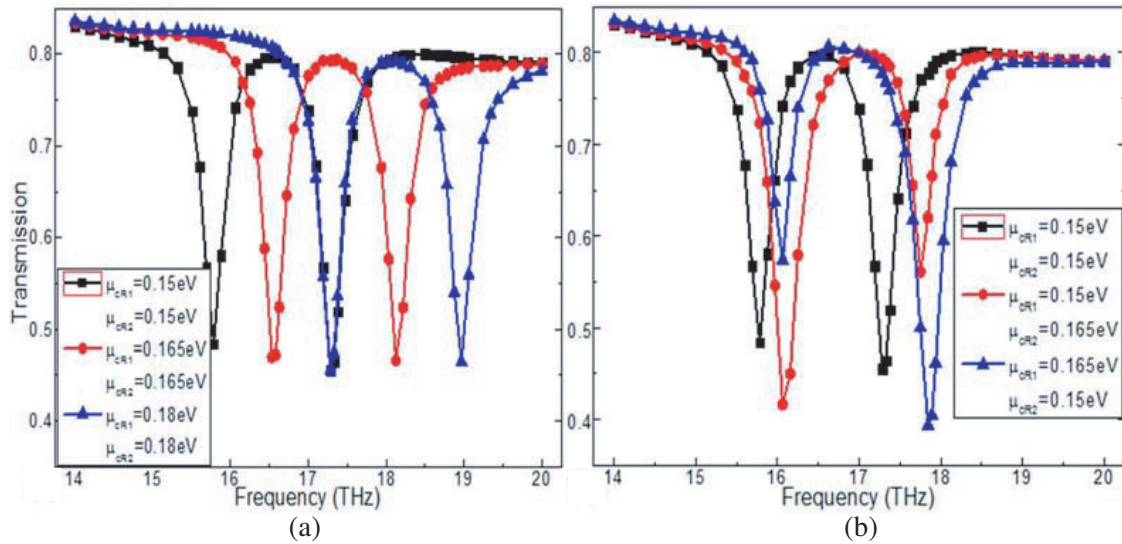


Figure 8. (a) Transmission spectra with $\mu_{cR1} = \mu_{cR2} = 0.15, 0.165,$ and 0.18 eV. (b) Transmission spectra with the chemical potential of 0.15 and 0.165 eV. The other parameters are the same as Fig. 7.

4. CONCLUSION

In conclusion, a compact graphene-based PIT structure is proposed and numerically investigated at THz and mid-infrared frequencies, which is composed of a graphene waveguide and two nanoribbon resonators. The common three-level atom system method is used to explore the physical origin of the behavior that causes the destructive interference of the two resonators. The novelty of this paper is that the PIT at different modes can be excited or suppressed by adjusting the proper coupling position between the two resonators. The performances of the PIT structure are analyzed at different coupling distance and chemical potentials. The proposed graphene-based PIT structure will have potential prospect in the field of nanoscale optical switching, nanolaser, and slow-light devices in the future.

ACKNOWLEDGMENT

This work was supported by the National Natural Science Foundation of China (61503219).

REFERENCES

1. Boller, K. J., A. Imamoglu, and S. E. Harris, "Observation of electromagnetically induced transparency," *Phys. Rev. Lett.*, Vol. 66, 2593, 1991.
2. Fleischhauer, M., A. Imamoglu, and J. P. Marangos, "Electromagnetically induced transparency: Optics in coherent media," *Rev. Mod. Phys.*, Vol. 77, 633–673, 2005.
3. Xu, Q., S. Sandhu, M. L. Povinelli, J. Shakya, S. Fan, and M. Lipson, "Experimental realization of an on-chip all-optical analogue to electromagnetically induced transparency," *Phys. Rev. Lett.*, Vol. 96, 123901, 2006.
4. Pappasimakis, N., V. A. Fedotov, N. I. Zheludev, and S. L. Prosvirnin, *Phys. Rev. Lett.*, Vol. 101, 253903, 2008.
5. Zhang, S., D. A. Genov, Y. Wang, M. Liu, and X. Zhang, "Plasmon-induced transparency in metamaterials," *Phys. Rev. Lett.*, Vol. 101, No. 4, 047401, 2008.
6. Liu, N., T. Weiss, M. Mesch, L. Langguth, U. Eigenthaler, M. Hirscher, C. Sönnichsen, and H. Giessen, "Planar metamaterial analogue of electromagnetically induced transparency for plasmonic sensing," *Nano Lett.*, Vol. 10, No. 4, 1103–1107, 2010.
7. Smith, D. D., H. Chang, K. A. Fuller, A. T. Rosenberger, and R. W. Boyd, "Coupled resonator induced transparency," *Phys. Rev. A*, Vol. 69, No. 6, 063804, 2004.
8. Xu, Q., S. Sandhu, M. L. Povinelli, J. Shakya, S. Fan, and M. Lipson, "Experimental realization of an on-chip all-optical analogue to electromagnetically induced transparency," *Phys. Rev. Lett.*, Vol. 96, No. 12, 123901, 2006.
9. Kekatpure, R. D., E. S. Barnard, W. Cai, and M. L. Brongersma, "Phase-coupled plasmon induced transparency," *Phys. Rev. Lett.*, Vol. 104, No. 24, 243902, 2010.
10. Wang, G., H. Lu, and X. Liu, "Dispersionless slow light in MIM waveguide based on a plasmonic analogue of electromagnetically induced transparency," *Opt. Express*, Vol. 20, 20902, 2012.
11. Lu, H., X. Liu, and D. Mao, "Plasmonic analog of electromagnetically induced transparency in multi-nanoresonator-coupled waveguide systems," *Phys. Rev. A*, Vol. 85, 053803, 2012.
12. Yahiaoui, R., K. Takano, F. Miyamaru, M. Hangyo, and P. Mounaix, "Terahertz meta-molecules deposited on thin flexible polymer: Design, fabrication and experimental characterization," *J. Opt.*, Vol. 16, 094014, 2014.
13. Yahiaoui, R., S. Tan, L. Cong, R. Singh, F. Yan, and W. Zhang, "Multispectral terahertz sensing with highly flexible ultrathin metamaterial absorber," *J. Appl. Phys.*, Vol. 118, 083103, 2015.
14. Yahiaoui, R., A. C. Strikwerda, and P. U. Jepsen, "Terahertz plasmonic structure with enhanced sensing capabilities," *IEEE Sensors Journal*, Vol. 16, 2484, 2016.
15. Barnes, W. L., A. Dereux, and T. W. Ebbesen, "Surface plasmon subwavelength optics," *Nature*, Vol. 424, 824–830, 2003.
16. He, X., Q. Wang, and S. F. Yu, "Investigation of multilayer subwavelength metallic-dielectric stratified structures," *IEEE J. Quantum Elect.*, Vol. 48, 1554, 2012.
17. Barnes, W. L., A. Dereux, and T. W. Ebbesen, "Surface plasmon subwavelength optics," *Nature*, Vol. 424, 824–830, 2003.
18. He, S., X. Zhang, and Y. He, "Graphene nano-ribbon waveguides of record-small mode area and ultra-high effective refractive indices for future VLSI," *Opt. Express*, Vol. 21, 30664–30673, 2013.
19. Nikitin, A. Y., F. Guinea, F. J. García-Vidal, and L. Martín-Moreno, "Edge and waveguide terahertz surface plasmon modes in graphene microribbons," *Phys. Rev. B*, Vol. 84, 161407, 2011.
20. Zhu, X., W. Yan, N. A. Mortensen, and S. Xiao, "Bends and splitters in graphene nanoribbon waveguides," *Opt. Express*, Vol. 21, 3486–3491, 2013.

21. Shi, X., D. Han, Y. Dai, Z. Yu, Y. Sun, H. Chen, X. Liu, and J. Zi, "Plasmonic analog of electromagnetically induced transparency in nanostructure graphene," *Opt. Express*, Vol. 21, No. 23, 28438, 2013.
22. Shi, X., X. Su, and Y. Yang, "Enhanced tunability of plasmon induced transparency in graphene strips," *J. Appl. Phys.*, Vol. 117, 143101, 2015.
23. Lin, Q., X. Zhai, L. Wang, B. Wang, G. Liu, and S. Xia, "Combined theoretical analysis for plasmon-induced transparency in integrated graphene waveguides with direct and indirect couplings," *EPL*, Vol. 111, 340004, 2015.
24. Wang, L., W. Li, and X. Jiang, "Tunable control of electromagnetically induced transparency analogue in a compact graphene-based waveguide," *Opt. Lett.*, Vol. 40, No. 10, 2325–2328, 2015.
25. Fu, G., X. Zhai, H. J. Li, S. X. Xia, and L. L. Wang, "Tunable plasmon-induced transparency based on bright-bright mode coupling between two parallel graphene nanostrips," *Plasmonics*, 2016, doi:10.1007/s11468-016-0215-4 (2016).
26. Wang, B., X. Zhang, X. Yuan, and J. Teng, "Optical coupling of surface plasmons between graphene sheets," *Appl. Phys. Lett.*, Vol. 100, 131111, 2012.
27. Gan, C. H., H. S. Chu, and E. P. Li, "Synthesis of highly confined surface plasmon modes with doped graphene sheets in the midinfrared and terahertz frequencies," *Phys. Rev. B*, Vol. 85, 125431, 2012.
28. Zhuang, H., F. Kong, K. Li, and S. Sheng, "Plasmonic bandpass filter based on graphene nanoribbon," *Appl. Opt.*, Vol. 54, 2558–2564, 2015.
29. Han, Z. H. and S. I. Bozhevolnyi, "Plasmon-induced transparency with detuned ultracompact Fabry-Perot resonators in integrated plasmonic devices," *Opt. Express*, Vol. 19, 3251–3257, 2011.